IOP Publishing | Institute of Physics and Engineering in Medicine Physics in Medicine & Biology

Phys. Med. Biol. **59** (2014) 6061–6084 doi:10.1088/0031-9155/59/20/6061

Application of adaptive kinetic modelling for bias propagation reduction in direct 4D image reconstruction

F A Kotasidis[1,2], J C Matthews[2], A J Reader[3,4], G I Angelis[5] and H Zaidi[1,6,7]

[1] Division of Nuclear Medicine and Molecular Imaging, Geneva University Hospital, CH-1211 Geneva, Switzerland
[2] Wolfson Molecular Imaging Centre, MAHSC, University of Manchester, M20 3LJ, Manchester, UK
[3] Department of Biomedical Engineering, Division of Imaging Sciences and Biomedical Engineering, King's College London, St. Thomas' Hospital, SE1 7EH, London, UK
[4] Montreal Neurological Institute, McGill University, QC H3A 2B4, Montreal, Canada
[5] Faculty of Health Sciences, Brain and Mind Research Institute, University of Sydney, NSW 2006, Australia
[6] Geneva Neuroscience Centre, Geneva Ussniversity, CH-1205 Geneva, Switzerland
[7] Department of Nuclear Medicine and Molecular Imaging, University of Groningen, University Medical Center Groningen, 9700 RB, Groningen, The Netherlands

E-mail: fotis.kotasidis@unige.ch

Received 22 April 2014, revised 5 August 2014
Accepted for publication 8 August 2014
Published 25 September 2014

Abstract

Parametric imaging in thoracic and abdominal PET can provide additional parameters more relevant to the pathophysiology of the system under study. However, dynamic data in the body are noisy due to the limiting counting statistics leading to suboptimal kinetic parameter estimates. Direct 4D image reconstruction algorithms can potentially improve kinetic parameter precision and accuracy in dynamic PET body imaging. However, construction of a common kinetic model is not always feasible and in contrast to post-reconstruction kinetic analysis, errors in poorly modelled regions may spatially propagate to regions which are well modelled. To reduce error propagation from erroneous model fits, we implement and evaluate a new approach to direct parameter estimation by incorporating a recently proposed kinetic modelling strategy within a direct 4D image reconstruction framework. The algorithm uses a secondary more general model to allow a less constrained model fit in regions where the kinetic model does not accurately describe the

underlying kinetics. A portion of the residuals then is adaptively included back into the image whilst preserving the primary model characteristics in other well modelled regions using a penalty term that trades off the models. Using fully 4D simulations based on dynamic [^{15}O]H_2O datasets, we demonstrate reduction in propagation-related bias for all kinetic parameters. Under noisy conditions, reductions in bias due to propagation are obtained at the cost of increased noise, which in turn results in increased bias and variance of the kinetic parameters. This trade-off reflects the challenge of separating the residuals arising from poor kinetic modelling fits from the residuals arising purely from noise. Nonetheless, the overall root mean square error is reduced in most regions and parameters. Using the adaptive 4D image reconstruction improved model fits can be obtained in poorly modelled regions, leading to reduced errors potentially propagating to regions of interest which the primary biologic model accurately describes. The proposed methodology, however, depends on the secondary model and choosing an optimal model on the residual space is critical in improving model fits.

Keywords: PET, direct 4D reconstruction, kinetic modelling, parametric imaging

(Some figures may appear in colour only in the online journal)

1. Introduction

PET has the inherent ability to detect and quantify changes in the bio-distribution of an intravenously administered radio-labelled tracer, through dynamic image acquisition of the system under study. By modelling the temporal distribution of the tracer, parameters of interest regarding specific biological processes can be derived. Traditionally, parametric imaging is performed by independently reconstructing a set of dynamic images, followed by kinetic analysis at the voxel level. However this approach suffers from reduced signal-to-noise ratio (SNR), resulting in noisy and biased parameter estimates. Different algorithms have been proposed for direct parameter estimation during image reconstruction in an attempt to improve SNR (Rahmim *et al* 2009). These algorithms, similar to the post-reconstruction analysis, make use of common image reconstruction algorithms which have been extended to accommodate either linear or non-linear kinetic models. Linear parametric image reconstruction can be based either on data driven methods, to describe the temporal distribution of the radioactivity concentration using a spectrum of temporal basis functions (Matthews *et al* 1997, Reader *et al* 2006), or make use of graphical analysis techniques such as the Patlak and Logan plots, to derive macro-parameters of interest (Tsoumpas *et al* 2008, Wang *et al* 2008, Rahmim *et al* 2012, Merlin *et al* 2013, Tang *et al* 2010) On the other hand, direct 4D image reconstruction based on non-linear models can deliver micro-parameters of interest, such as rate constants between blood and tissue (Kamasak *et al* 2005, Jianhua *et al* 2012, Rakvongthai *et al* 2013). However these are usually complex due to the non-linear estimation of parameter and computationally demanding making them impractical for clinical issue. One complication common in both linear and non-linear parametric image reconstruction algorithms is that due to the respective coupling between the spatial model and the temporal model, these algorithms can suffer from slow convergence and can be trapped to local maxima due to the objective function no longer being concave. These algorithms are also restricted to a specific combination of spatial and temporal model while incorporation

of certain temporal models within a 4D reconstruction framework is not straightforward. To overcome these difficulties an optimization transfer approach can be used to decouple the tomographic from the kinetic parameter estimation problem in every iteration, using an algorithm which resembles the post-reconstruction parameter estimation approach, but converges to the solution of the 4D spatiotemporal problem (Wang and Qi 2009, Matthews *et al* 2010, Wang and Qi 2010, Rahmim *et al* 2011, Wang and Qi 2012). By using the optimization transfer approach based on surrogate functions, the 4D maximum likelihood problem is converted into a tomographic and an image based fitting problem. The benefit of such an approach is that well established kinetic modelling algorithms can be used to solve the parameter estimation problem.

Direct 4D image reconstruction methods have been shown to improve bias and variance in parameter estimates when applied to brain imaging studies. However so far their application to dynamic body imaging has been limited (Kotasidis *et al* 2010, Rahmim *et al* 2010, Kotasidis *et al* 2012, Su *et al* 2013, Rahmim *et al* 2014). This is partly due to the multitude of organ structures and regions with diverse kinetics, making kinetic modelling in the body challenging and its application within a 4D framework particularly complex. Regions with differential delay and dispersion (thoracic versus abdominal organs as well as veins carrying the activity from the injection site) and activity delivery through routes other than arterial blood (such as urinary excretion, bile, as well as venous delivery in the liver), can be located within the FOV. In such cases, a single model cannot always describe the kinetics within the FOV. This is in contrast to brain imaging, where using a single model to describe the underlying temporal distribution of a given tracer is usually a valid approximation, with activity arriving through the carotid arteries and with a small differential delay and dispersion in the different brain regions. However even in the brain, delivery of activity through cerebrospinal fluid could potentially complicate the underlying kinetics and make the construction of a common kinetic model not feasible.

In conventional post-reconstruction kinetic analysis, a model which adequately describes the regions of primary interest is selected in most cases, with the remainder of the regions being poorly modeled. Thus parametric maps with meaningful kinetic parameters can be obtained in regions for which the model accurately describes the underlying kinetics. In the remainder of the regions, where the model is expected to provide poor fits to the dynamic data, kinetic parameters can simply be ignored. Contrary to post-reconstruction analysis, where erroneous kinetic modelling results in localized kinetic parameter bias, in direct 4D methods errors from discrepancies between the measured and modeled data during the kinetic modelling step can spatially propagate during the tomographic step (Kotasidis *et al* 2011). This results in bias propagating from poorly modeled regions, to regions where the kinetic model accurately describes the underlying kinetics. This in turn reduces the benefits of direct 4D methods in regions affected by error propagation or even producing more biased kinetic parameter estimates than conventional post-reconstruction methods.

Due to the interleaving between the tomographic and the kinetic modelling steps that is used in the 4D framework it is apparent that in order to avoid bias from poorly modeled regions spatially propagating to regions which are of interest, it is imperative that the kinetics of all regions in the FOV are accurately described. Thus good data fits both in well and poorly modelled regions should be obtained after kinetic modelling between tomographic iterations. However in conventional 4D reconstruction schemes, similar to post-reconstruction techniques, a single model is applied in the entire image volume to generate direct parametric maps.

In this work, we implement and evaluate a new approach to direct 4D reconstruction in order to reduce error propagation from poorly modelled regions. The method is based on the application of a recently proposed post-reconstruction adaptive kinetic modelling

methodology (Matthews *et al* 2012). This adaptive scheme introduces a primary biologic model to derive meaningful kinetic parameters in the regions of interest whilst allowing a less constrained fit in regions where the primary model doesn't fit the data via a penalised secondary model. Direct 4D image reconstruction based on surrogate functions and optimization transfer allow existing kinetic modelling parameter estimation algorithms to be utilized. Thus the proposed methodology can be implemented within a 4D framework in a relative straightforward way, by iteratively fitting the adaptive model after every tomographic update. The new direct 4D image reconstruction method is compared against conventional 4D reconstruction as well as post-reconstruction kinetic analysis, using noiseless as well as noisy fully 4D simulated data.

2. Theory

As mentioned earlier, a number of direct 4D kinetic parameter estimation schemes have been introduced based on separation between the tomographic and the image-based kinetic model problems. This approach has significantly simplified the previously complex and kinetic model specific optimization algorithms. Furthermore these schemes generalized the parameter estimation step by allowing the algorithm to be adapted to the different kinetic models.

The proposed method is an extension of a previously introduced 4D expectation maximization (EM) algorithm for direct kinetic parameter estimation (Matthews *et al* 2010). This algorithm herein referred to as the conventional 4D reconstruction method, is based on converting the spatiotemporal 4D maximum likelihood problem in projection space,

$$\alpha^{opt} = \underset{\alpha}{\operatorname{argmax}} \sum_{il} \left(m_{il} \log_e (y_{il}) - y_{il} \right) \tag{1}$$

$$y_{il} = \sum_j p_{ij} \lambda_{jl} + \eta_{il} = \sum_j p_{ij} f_{jl}(\alpha) + \eta_{il} \tag{2}$$

where during the l^{th} time frame and in the i^{th}data bin, $m_{il}$are the PET measured data, $y_{il}$the mean number of expected events, η_{il} the mean number of erroneous events, $p_{ij}$the probability system matrix of a photon emitted from the j^{th} voxel and being detected in the i^{th} projection bin and λ_{jl} is the number of emissions from the j^{th} voxel in the image during the l^{th} time frame described by a kinetic model f_{jl} with parameter vector α; into a maximum likelihood problem in image space

$$\alpha^{(k+1)} = \underset{\alpha}{\operatorname{argmax}} \sum_j \left(\sum_i p_{ij} \right) \sum_l \left(\lambda_{jl}^{(k+1)} \log_e \left(f_{jl}(\alpha) \right) - f_{jl}(\alpha) \right) \tag{3}$$

where

$$\lambda_{jl}^{(k+1)} = \frac{f_{jl}(\alpha^{(k)})}{\sum_i p_{ij}} \sum_i \frac{p_{ij} y_{il}}{\sum_{j'} p_{ij'} f_{j'l}(\alpha^{(k)}) + \eta_{il}} \tag{4}$$

Using a one step late approach equation (3) can be approximated with a weighted least square problem

$$\alpha^{(k+1)} = \underset{\alpha}{\operatorname{argmin}} \frac{1}{2} \sum_{jl} w_{jl}(\alpha) \left(\lambda_{jl}^{(k+1)} - f_{jl}(\alpha) \right)^2 \tag{5}$$

where the weights are given by

$$w_{jl}(\alpha) = \frac{1}{f_{jl}(\alpha)} \tag{6}$$

with k being the number of iterations.

The algorithm proceeds by alternating between the tomographic EM image update (equation (4)) and the voxel wise image-based least squares kinetic modelling steps (equation (5)). This algorithmic sequence resembles the post-reconstruction parameter estimation routine as kinetic modelling is performed on the current multiframe image estimate in the image domain but delivers direct parameter estimates, with parameter estimation performed between tomographic updates.

When construction of a common simple kinetic model within the imaging FOV is ensured, the aforementioned direct EM 4D framework can deliver parametric maps of improved precision and accuracy compared to post-reconstruction kinetic analysis. This has been demonstrated for both 1-tissue (Kotasidis *et al* 2010), irreversible 2-tissue (Angelis *et al* 2014, Kotasidis *et al* 2012) and reversible simplified reference tissue models (Gravel and Reader 2013), in perfusion, metabolism and brain imaging studies respectively. However in the presence of complex kinetics in the FOV, due to the inability to construct a common kinetic framework, model fitting errors in poorly modelled regions could potentially spatially propagate in other well modelled regions, resulting in biased parameter estimates (Kotasidis *et al* 2011).

The new adaptive 4D image reconstruction algorithm utilizes a recently proposed generic kinetic model strategy during the kinetic modelling step, to allow good full FOV model fitting in the presence of complex kinetics. The method is based on the application of a primary biologic kinetic model and a secondary more general model (Matthews *et al* 2012). Since the primary biologic model is preferred to generate the parametric maps, the secondary model should be penalised.

If linear models are considered, let $\lambda = \mathrm{A}\alpha$ be the primary biologic model, where λ is the activity concentration vector over the duration of the scan for a number of l time frames and α is the vector holding the model parameters. And let $\lambda = \mathbf{Bz}$ be a secondary model to describe kinetics not modelled by the primary model, where z similarly holds the secondary model parameters and which is penalised such that

$$\alpha^{opt}, z^{opt} = \underset{\alpha,z}{\operatorname{argmin}} \begin{pmatrix} (\mathbf{A}\alpha + \mathbf{B}z - \lambda)^T \mathbf{W} (\mathbf{A}\alpha + \mathbf{B}z - \lambda) + \\ \beta z^T \mathbf{B^T W B} z \end{pmatrix} \tag{7}$$

Setting $\mathbf{B^T W A} = 0$ to impose an orthogonality between the spaces described by the 2 models and avoid the dependency of the primary model parameters on the penalty term β, the solution of equation (7) is

$$\begin{aligned} &\alpha^{opt} = (\mathbf{A}^T\mathbf{W}\mathbf{A})^{-1}\mathbf{A}^T\mathbf{W}\lambda \\ &\text{and} \\ &z^{opt} = \frac{1}{1+\beta}(\mathbf{B}^T\mathbf{W}\mathbf{B})^{-1}\mathbf{B}^T\mathbf{W}\mathbf{r} \end{aligned} \tag{8}$$

where

$$\mathbf{r} = (\mathbf{I} - \mathbf{A}(\mathbf{A}^T\mathbf{W}\mathbf{A})^{-1}\mathbf{A}^T\mathbf{W})\lambda \tag{9}$$

are the residuals following primary model fitting.

This penalised 2 tier kinetic model framework leads then to a simple two step approach as described in detail in (Matthews *et al* 2012):

1) fit the primary model to the data to generate kinetic parameters:
2) fit the secondary model on the residuals resulting after primary model fitting:
3) construct the new data estimate based on the evaluation of the primary model adding a fraction of the residuals modelled by the secondary model.

$$\lambda^{est} = \mathbf{A}\alpha^{opt} + \frac{1}{1+\beta}\mathbf{B}\mathbf{z}^{opt} \tag{10}$$

Extending the above formulation to non-linear kinetic models the image estimate becomes:

$$\lambda^{est} = f(\alpha^{opt}) + \frac{1}{1+\beta}h(\mathbf{z}^{opt}) \tag{11}$$

where $\lambda = f(\alpha)$ and $\lambda = h(\mathbf{z})$ are the primary and secondary non-linear models respectively with parameter vectors α and z. For non-linear models and methods like the generalized linear least squares (GLLS) where the $\mathbf{A}$ matrices are different amongst voxels, the columns of $\mathbf{B}$ can no longer be guaranteed to be orthogonal to $\mathbf{A}$ with projection needed for each unique $\mathbf{A}$ matrix. So potentially a different secondary model is needed for each voxel or use a common secondary model and project this to be orthogonal to the primary model solution. However such a projection is not practical and computationally expensive within 4D reconstruction. Neglecting this projection will only result in a slightly more conservative approach with effectively having a smaller fraction of the residuals being fitted which is a small price to pay for avoiding such a projection in each voxel. An important parameter in this optimization is the penalty term β which controls the fraction $\left(\frac{1}{1+\beta}\right)$ of the secondary residual model fit to be included. We used a generalised crossed validation method to optimize β. Specifically the generalised cross validation determines the optimal value from

$$\begin{aligned} \beta^{opt} &= \underset{\beta}{\operatorname{argmin}}(V(\beta)) \\ V(\beta) &= \frac{\mathbf{y}^T(\mathbf{I}_n - \mathbf{T}(\beta))^T(\mathbf{I}_n - \mathbf{T}(\beta))\mathbf{y}}{(Tr(\mathbf{I}_n - \mathbf{T}(\beta)))^2} = \frac{RSS(\beta)}{(df(\beta))^2} \end{aligned} \tag{12}$$

where $\mathbf{T}(\beta)$ is the influence matrix, the matrix that maps the measurements λ to the estimate $\lambda^{\mathbf{est}}$. Note that the matrix $\mathbf{I}_n - \mathbf{T}(\beta)$ maps the measured data $\mathbf{y}$ to the residuals so that the numerator is just the residual sum of squares. The trace of $\mathbf{I}_n - \mathbf{T}(\beta)$ can be thought of as the effective number of degrees of freedom

After evaluating equation (12) as described in (Matthews *et al* 2012) the portion of the residual fit to be included is given by:

$$\kappa = \left(\frac{1}{1+\beta^{opt}}\right) = \left[\frac{1 - \frac{r_{df}}{r_{RSS}}}{1 - r_{df}}\right]_+ \tag{13}$$

where $[\cdot]_+$ corresponds to truncation to positive values, r_{RSS} is the fraction of the residual sum of squares described by the secondary model and $r_{df}$is the ratio of the degrees of freedom in the secondary model to the remaining degrees of freedom after the application of the primary model.

The application of a secondary model on the residual space attempts to describe any structure or temporal correlation in the residuals, which could result from the application of an erroneous

primary kinetic model. If structured residuals are identified and modelled, then a portion of these is adaptively included back into the dynamic image sequence. The purpose of the additional secondary model fitting step is to improve fit in regions for which the primary model doesn't fit the data, without affecting the kinetic parameter estimated during the primary model fit. Thus in well modelled regions, meaningful parametric maps can be obtained. However, in poorly modelled regions, although the secondary model cannot alter the kinetic parameters estimated from the primary biologic model, it can improve on the fit of the time-activity curve (TAC) by allowing a portion of the residuals to be reintroduced back into the dynamic image sequence. Incorporating such a kinetic model strategy within 4D reconstruction could result in reduced fitting errors from discrepancies between the measured and modeled data attributed to erroneous model formulation, potentially minimizing their spatial propagation between the tomographic iterations. It has to be emphasized that the introduction of the secondary model does not affect the kinetic parameters estimated after the application of the primary model but it only improves the fit to the data. As such its potential benefit in the context of the 4D parameter estimation is indirect. The improved fitting in those erroneously modeled regions could minimize error propagation in the well modeled regions, allowing the 4D method to deliver its full potential.

Adding the adaptive kinetic model framework, in our existing 4D EM framework, the proposed algorithm executes as follows:

(i) Start with image estimate $\lambda_{jl}^{(k)}$:
(ii) Perform one image update over all temporal frames with conventional frame-by-frame ordered subsets expectation maximization algorithm (OSEM) using equation (4) to calculate $\lambda_{jl}^{(k+1)}$
(iii) Fit the primary kinetic model in image space (if model requires parameter initialization use uniform values or a parameter estimation method with no self-initialization during the 1st tomographic iteration with $\alpha^{(k)}$ as an initial estimate for subsequent tomographic iterations) and hence calculate parameters $\alpha^{(k+1)}$
(iv) Use the updated kinetic parameters to evaluate spatiotemporal 4D image $f_{jl}(\alpha^{(k+1)})$.
(v) Calculate primary model residuals $\lambda_{jl}^{(k+1)} - f_{jl}(\alpha^{(k+1)})$.
(vi) Fit secondary model on the residuals and calculate fraction of the fit to be included back in the image according to equation (13)
(vii) Evaluate the new fitted image $\lambda_{jl}^{(k+1)} = f_{jl}(\alpha^{(k+1)}) + \frac{1}{1+\beta_j^{opt}} h_{jl}(z^{(k+1)})$ and repeat from (ii)

In the absence of any erroneous model formulation residuals after the application of the primary model are attributed to noise. However in the case where an erroneous model is used to fit the data, both random and temporally correlated residuals coexist in the residual space. Choosing an appropriate secondary model is then paramount to be able to differentiate between structured residuals from erroneous biological model fitting and residuals originating from random noise. One option then is to use smooth basis functions such as polynomials, splines and low frequency sine functions (i.e. Fourier filtering), to capture the temporal dependency potentially from biological information that cannot be modelled by the primary model, with all approaches potentially promising. Such spaces defined by the columns of **B** will not necessarily be orthogonal to the space defined by **A** and hence will need to be projected prior to use. Another data driven approach, consists of decomposing the residuals and using the highest singular values as the secondary model matrix. This approach is based on the assumption that if there is a biological process not modelled by the primary model it is likely to exist in a number of image voxels. Hence there will be structure in the covariance matrix of the residuals. This construction has some convenient properties in that the space defined by the matrix **B** is already orthogonal to **A**.

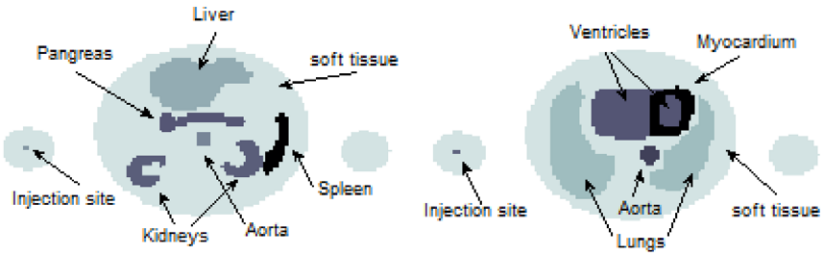

Figure 1. Representative phantom planes along with the different simulated regions.

Table 1. Simulated Kinetic parameters for the 10 regions used in the digital phantom from a typical [^{15}O]H_2O PET scan.

	K_1 ml/sec/ml	k_2 ml/sec/ml	Va ml/ml	Vd ml/ml
Kidneys	0.0250	0.0309	0.15	0.81
Spleen	0.0300	0.0319	0.55	0.94
Liver	0.0117	0.0119	0.05	0.98
Pancreas	0.0417	0.0484	0.10	0.86
Myocardium	0.0167	0.0183	0.15	0.91
Lungs	0.0008	0.0014	0.06	0.60
Soft tissue	0.0005	0.0042	0	0.12
Aorta	0	0	1	0
Injection	0	0	1	0
Ventricles	0	0	1	0

3. Methods

To evaluate the proposed algorithm, typical [^{15}O]H_2O kinetics were simulated using a 4D digital phantom, with time-activity curves (TACs) representing a 3 parameter 1-tissue model (K_1, k_2), including a blood volume component (bv).

$$C_{PET}(t) = K_1 C_a(t) \bigotimes e^{-(k_2)\cdot t} + bv \cdot C_a(t) \tag{14}$$

where C_a represents the input function.

Ten regions of interest were delineated on the phantom, representing major internal body structures. A CT scan from a healthy patient was used to extract the regions of interest (figure 1). In each region kinetic parameters from a typical [^{15}O]H_2O scan were assigned (table 1). Two dynamic datasets each simulating a typical 550MBq injected activity (210×10^6 prompts and 111×10^6 randoms) 6 min scan with 28 time frames (1×130 s, 14×5 s, 5×10 s, 3×20 s, 6×30 s), were generated, one with simple and one with more realistic and diverse kinetics (tables 2 and 3).

In the simple dataset that represents the reference against which the complex one is compared to, all organ regions shared a common input function (IF) using a single input model. The IF used to generate TACs in the different organ structures corresponds to the TAC used for the aorta, injection site and heart ventricles, as there is no tissue response in these regions and the TAC represents the blood volume component. In the complex dataset with diverse kinetics in the FOV, a differential delay and dispersion, representing earlier tracer arrival times, was used to generate the TACs in the injection site (delay = -16 s, dispersion coefficient = 0.08) and heart ventricles (delay = -8 s, dispersion coefficient = 0.09) compared to the aorta (dispersion coefficient = 0.1, considering the tracer's arrival time in the aorta as the reference zero time

Table 2. Input function supply, delay and blood volume parameters used for the kinetic model during generation of the simple dataset and for the kinetic model during parameter estimation for the 10 regions used in the digital phantom.

	Simulated Kinetics			Kinetic model			
Simple dataset	Input	d	bv	Input	d	bv	Match
Kidneys	Single	No	Yes	Single	No	Yes	Yes
Spleen	Single	No	Yes	Single	No	Yes	Yes
Liver	Single	No	Yes	Single	No	Yes	Yes
Pancreas	Single	No	Yes	Single	No	Yes	Yes
Myocardium	Single	No	Yes	Single	No	Yes	Yes
Lungs	Single	No	Yes	Single	No	Yes	Yes
Soft tissue	Single	No	No	Single	No	Yes	Yes
Aorta	Single	No	Yes	Single	No	Yes	Yes
Injection	Single	No	Yes	Single	No	Yes	Yes
Ventricles	Single	No	Yes	Single	No	Yes	Yes

Table 3. Input function supply, delay and blood volume parameters used for the kinetic model during generation of the complex dataset and for the kinetic model during parameter estimation for the 10 regions used in the digital phantom. Differences to the simple dataset are marked in bold.

	Simulated Kinetics			Kinetic model			
Complex dataset	Input	d	bv	Input	d	bv	Match
Kidneys	Single	No	Yes	Single	No	Yes	Yes
Spleen	Single	No	Yes	Single	No	Yes	Yes
Liver	**Dual**	No	Yes	Single	No	Yes	**No**
Pancreas	Single	No	Yes	Single	No	Yes	Yes
Myocardium	Single	No	Yes	Single	No	Yes	Yes
Lungs	Single	No	Yes	Single	No	Yes	Yes
Soft tissue	Single	No	No	Single	No	Yes	Yes
Aorta	Single	No	Yes	Single	No	Yes	Yes
Injection	Single	**Yes**	Yes	Single	No	Yes	**No**
Ventricles	Single	**Yes**	Yes	Single	No	Yes	**No**

point and similar to the simple dataset). In different organs the TAC in the aorta was used as an IF (again similar to the simple dataset). Furthermore a dual input model was used in the liver (hepatic artery + portal vein) (Kudomi *et al* 2008) compared to other regions (single input model). No attenuation, normalization and scatter effects were considered during the reconstruction. The dynamic images from both datasets were forward projected into a virtual scanner with the geometry configuration of the Siemens HiRez PET/CT scanner to create the dynamic projection datasets. Poisson noise was introduced and 50 noisy realizations were generated for each dataset.

Both datasets were then reconstructed using the adaptive 4D reconstruction, as well as conventional 4D reconstruction without adaptive modelling in order to generate parametric maps. 3D reconstruction followed by kinetic modelling was also used for comparison. For the primary kinetic model, we used a 3 parameter, 1-tissue single input model including a blood volume term, with no delay and dispersion in the IF (the IF is similar to the IF used to generate the data). As such the model is representative of all the regions in the simple dataset while in the complex dataset is representative of all regions apart from the injection site and heart ventricles due to mismatch in the delay and dispersion of the IF as well as the liver due to a dual input supply. The generalized linear least square (GLLS) method was used to generate parametric maps. The linear least square (LLS) method was used for the 1st iteration to

initialize the kinetic parameters for GLLS, since it requires no self-initialization as opposed to GLLS which requires initial parameter estimates (Feng *et al* 1996). In the adaptive 4D reconstruction, a data-driven method was used in order to generate the secondary residual model (Matthews *et al* 2012).

The covariance matrix of the residuals was decomposed using singular value decomposition and a number of singular values (SVs) were used to construct the secondary model. Varying number of SVs were used in order to assess the impact of the secondary model on bias propagation. The incentive behind using a data driven approach is that the model doesn't make a priori assumptions about the structure of the residuals resulting from the primary model fit such as temporal dependency. Instead it is based on the idea that a cluster of voxels are likely to exist in the presence of kinetics not modelled by the primary model (Matthews *et al* 2012). Hence there will be structure in the residual's covariance matrix.

4. Results

4.1. Impact of adaptive 4D reconstruction on time-activity curves

Figure 2 shows the simulated TACs as well as the TACs before and after the kinetic modelling step using post-reconstruction kinetic analysis (a), conventional 4D reconstruction (b) and the proposed adaptive 4D reconstruction (c), at the 15th tomographic iteration (21 subsets) and for noiseless data. TACs are taken from the complex dataset and include both badly modelled (injection site, ventricles and liver) as well as representative well modelled regions (pancreas, myocardium). Looking at the post-reconstruction analysis, the TACs corresponding to the well modelled regions, before and after kinetic modelling, coincide with the simulated TACs, since there is a good match between the simulated kinetics and the model used for parameter estimation. In the badly modelled regions however, a bad fit is obtained owing to the model used for parameter estimation, which is not representative of the simulated kinetics. The TACs in the injection site and ventricles are shifted due to the erroneous delay used, while the liver TAC is biased due to using a single input model as opposed to a dual input model. Moving to the conventional 4D reconstruction, in the badly modelled regions the TACs are biased even before the kinetic modelling step. This is due to the fact that the TACs are shown at the 15th iteration and with the 4D reconstruction alternating between the tomographic and kinetic modelling steps, the erroneous model has been applied in these regions multiple times. Also looking at the well modelled regions, the TACs before and after the kinetic modelling step no longer coincide with the simulated ones. This is due to bias from badly modelled regions propagating during the previous iterations in these well-modelled regions, creating bias in the parameter estimates during kinetic modelling and as a consequence biased TACs. Finally looking at the proposed adaptive method, the TACS in the badly regions coincide with the simulated TACs. As such, using adaptive modelling, TACs from badly modelled regions are no longer biased after the kinetic modelling step and as a consequence no bias is propagating to well modelled regions during the tomographic step.

4.2. Impact of adaptive 4D reconstruction on the spatial propagation of model induced bias - noiseless data

To evaluate the effect of the proposed algorithm on the kinetic parameters, parametric images of bias for 3 parameters and for both simulated datasets are shown in figure 3 (15 iterations - 21 subsets). In the simple dataset where there is a good match between the simulated and modelled kinetics, the adaptive 4D reconstruction (figure 3 (iii)) delivers parametric maps with almost

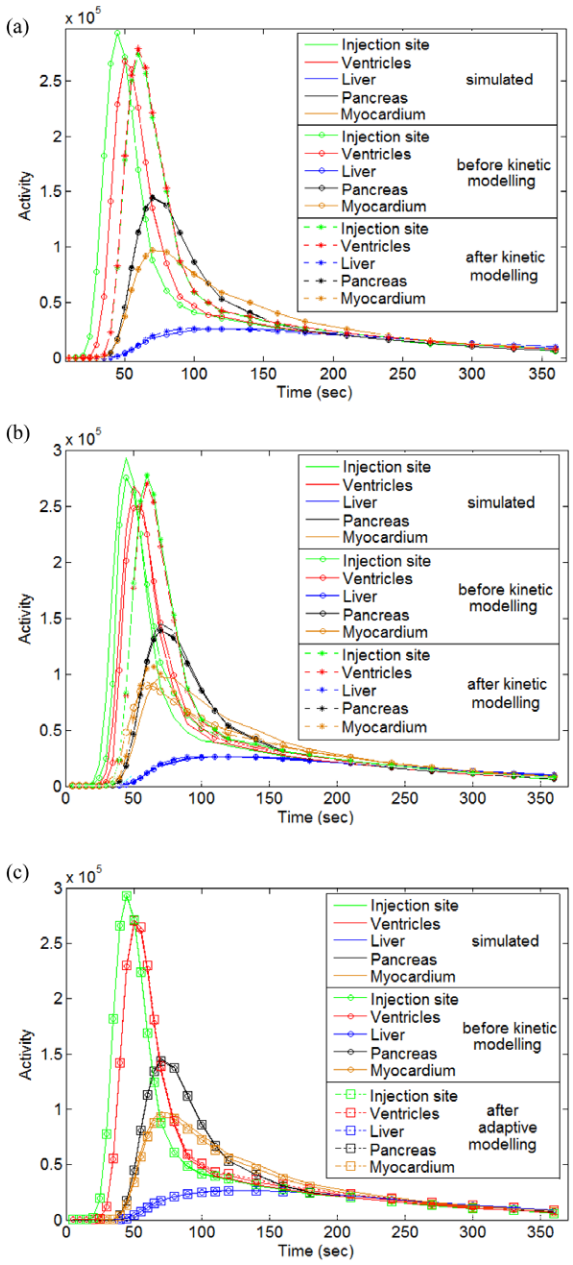

Figure 2. (*a*) TACs from the complex dataset for the post-reconstruction kinetic analysis, and (*b*) conventional 4D reconstruction curves (before kinetic modelling (after step (ii)) and after kinetic modelling (after step (iv))) as well as (*c*) for the adaptive 4D reconstruction (before kinetic modelling (after step (ii)) and after adaptive kinetic modelling (after step (vii))) all at the 15th iteration (21 subsets).The TACs (noiseless data) are shown for badly modelled regions (injection site, ventricles and liver) and 2 well-modelled regions (pancreas and myocardium). Using the adaptive 4D method, the TACs from the badly modelled regions match the simulated ones after using a secondary model to model the residuals, ensuring a good fit to the data even though the primary model results in a bad fit in these regions.

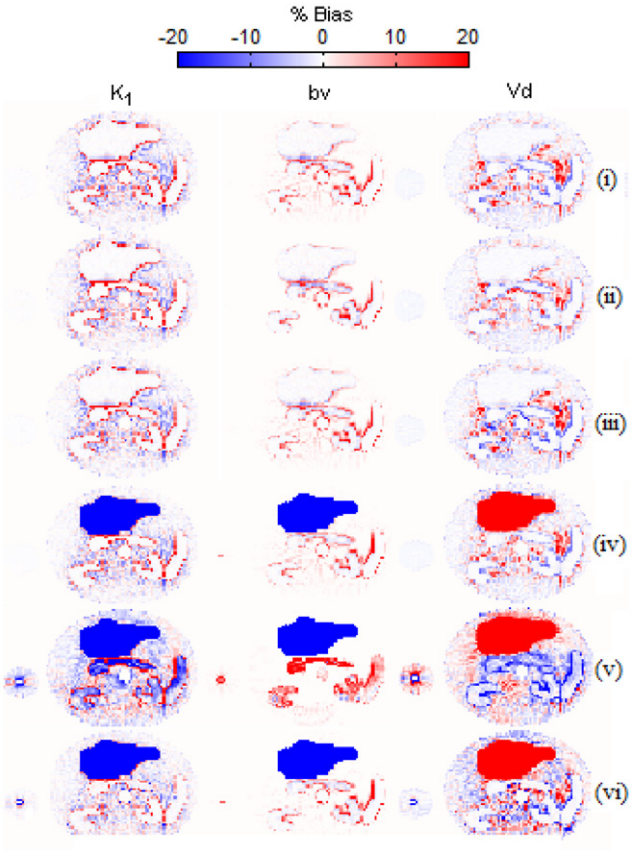

Figure 3. Parametric images of K_1, blood volume (bv) and Vd bias for the simple (i-iii) and complex noiseless datasets (iv-vi) using post-reconstruction kinetic modelling (i,iv), conventional 4D image reconstruction (ii, v) and the proposed adaptive 4D reconstruction (iii, vi). In the adaptive method 4 singular values are used in the secondary model.

zero bias in all parameters, similar to the results obtained by the post-reconstruction kinetic analysis (figure 3 (i)). As all regions are well modelled in this dataset and no structured residuals exist after the kinetic modelling step, the adaptive 4D reconstruction behaves similarly to the conventional 4D reconstruction (figure 3 (ii)). When there are complex kinetics in the FOV and there is a discrepancy between the simulated and modelled kinetics (in the injection site, ventricles and liver), the conventional 4D reconstruction (figure 3 (v)) delivers biased parametric maps contrary to the post-reconstruction (figure 3 (iv)), where errors are localized as was also reported in (Kotasidis *et al* 2011). Using the proposed adaptive 4D, the bias maps appear to be substantially improved (figure 3 (vi)). Bias in the vicinity of the liver (spleen, pancreas and kidneys) and injection is almost completely eradicated and resembling the post-reconstruction parametric maps with the bias localised in the liver and injection site (figure 3 (iv)).

4.3. Impact of the secondary model on residuals and spatial propagation of model induced bias–noiseless data

One parameter that is crucial in trying to identify and model structure residuals as opposed to noise, is the choice of the secondary model and its dimensionality. In figure 4 parametric

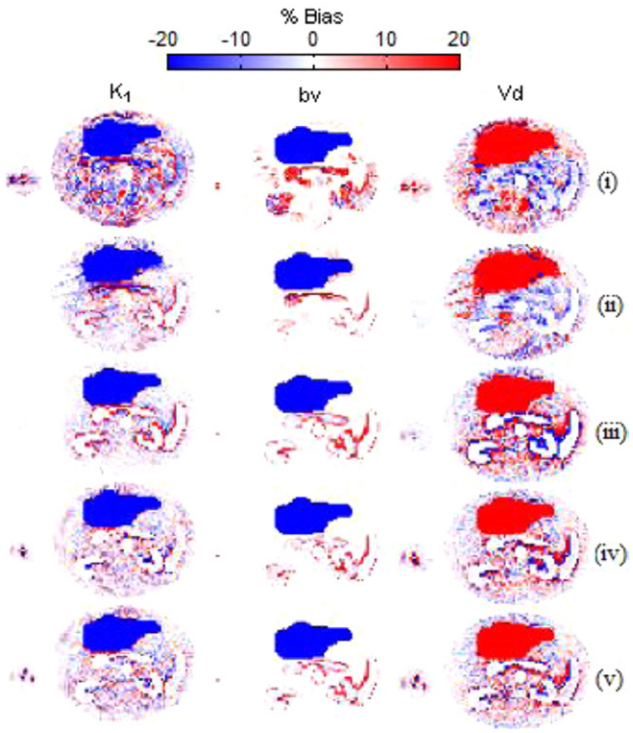

Figure 4. Parametric images of K_1, blood volume and Vd bias for the complex dataset obtained with the proposed adaptive 4D image reconstruction using an increasing number of singular values (1 SVs (i), 2 SVs (ii), 3 SVs (iii), 5 SVs (iv) and 8 SVs (v)) for the secondary model (noiseless data).

images of bias are shown for K_1, blood volume and Vd for the complex dataset, where there are structured residuals, using an increasing number of SVs as a secondary model space (15 iterations - 21 subsets). Using only the first singular value doesn't result in improvement in the parameter estimates, with bias propagation still affecting the well-modelled regions. When 2 SVs are used bias propagation is substantially reduced with bias only localized in the badly modelled regions, while further improvements are obtained when using 3. This is due to the fact that as more singular values are included in the secondary model, the structured residuals are more accurately described by the secondary model. Quantitative evaluation is shown in figure 5 where K_1 (a) and Vd (b) bias is plotted as a function of iterations for all reconstruction methods, for a region of interest in the pancreas (well-modelled region) from the complex dataset. Negative bias is seen in both K_1 and Vd in the conventional 4D reconstruction due to propagation from badly modelled regions. Using the adaptive 4D method, the bias due to propagation is progressively reduced as more singular values are included in the secondary model, approaching the zero bias seen in the post-reconstruction analysis. Similar improvements are obtained in blood volume where the positive bias observed in figure 4 is progressively reduced with singular values This trend observed in all parameters is reflected in figure 6, where images of the residual sum of squares (RSS) corresponding to the parametric images of figure 4 are shown, before the adaptive modelling (after fitting the primary model) and after the adaptive modelling (after using the secondary model and putting a portion of the residuals back into the dynamic image sequence) at the 15th iteration. When the first 2

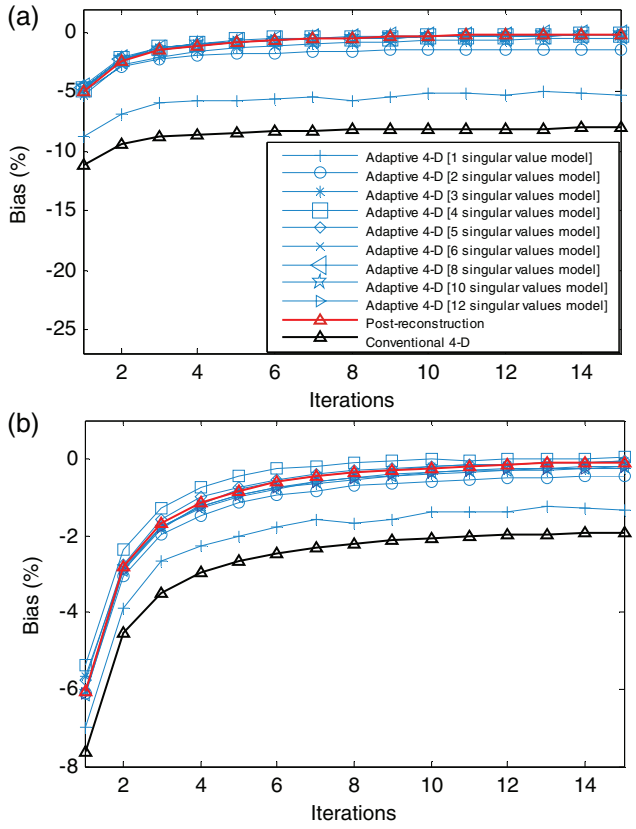

Figure 5. Bias as a function of iterations for K_1 (*a*) and Vd (*b*) for a region of interest covering the entire pancreas (well-modelled region from the complex dataset) for all parameter estimation methods (noiseless data). As more singular values are used for the secondary model in the adaptive method, bias due to propagation converges to zero, similar to post-reconstruction kinetic analysis.

singular values are used for the secondary model (figure 6 (ii,iii)), only a small portion of the structured residuals is modelled, with the RSS being similar before and after the adaptive modelling. As more singular values are used, structured residuals are only visible in the badly modelled regions looking before the application of the adaptive modelling, with the well modelled regions having no residuals due to propagation. This is due to the fact that even though the RSS is shown before the adaptive modelling for that tomographic iteration, the adaptive modelling has been applied multiple times during the previous iterations. After the adaptive modelling no structured residuals exist both in the well and badly-modelled regions meaning that a good fit is obtained in all image voxels. Similar to figure 5, the mean K_1 and Vd bias is plotted in figure 7, for all regions of interest (ROIs) in the complex dataset and for all the parameter estimation methods (15th iteration). Bias originating from the liver is propagating to most of the regions in the conventional 4D reconstruction which slowly converges towards zero bias using the adaptive method with 3 SVs. However some regions such as the myocardium, being close to sizable badly modelled regions with large errors (heart ventricles) suffer from excessive bias which although substantially improved in the adaptive 4D method, fluctuates with the number of SVs. Finally bias in the liver, representing a poorly modelled regions,

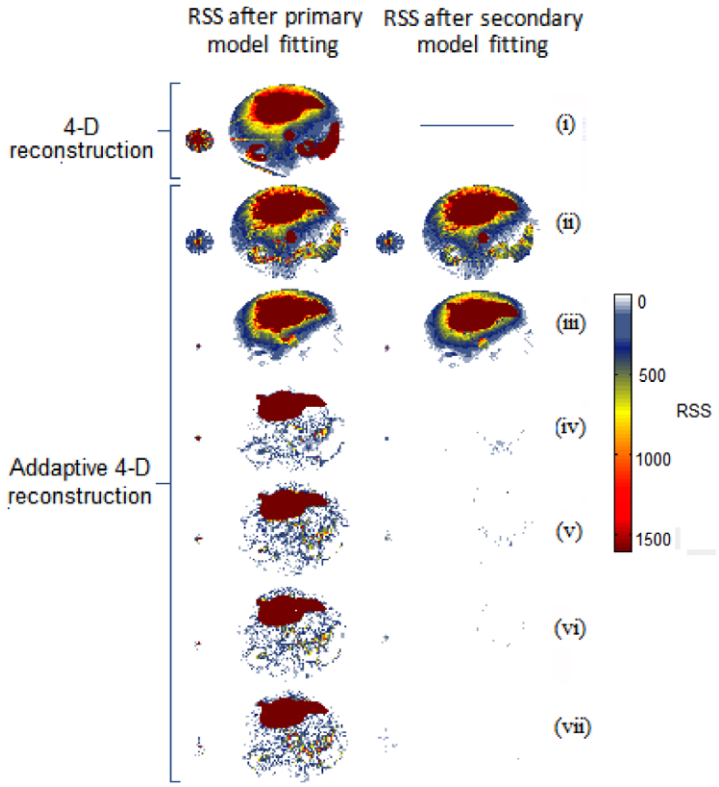

Figure 6. Parametric images of the residual sum of squares for the complex dataset (noiseless data) before and after adaptive modelling at the 15th tomographic iteration using an increasing number of singular values for the secondary model space (1 SVs (ii), 2 SVs (iii), 3 SVs (iv), 5 SVs (v) and 8 SVs (vi)). The residual sum of squares for the conventional 4D method is shown for comparison.

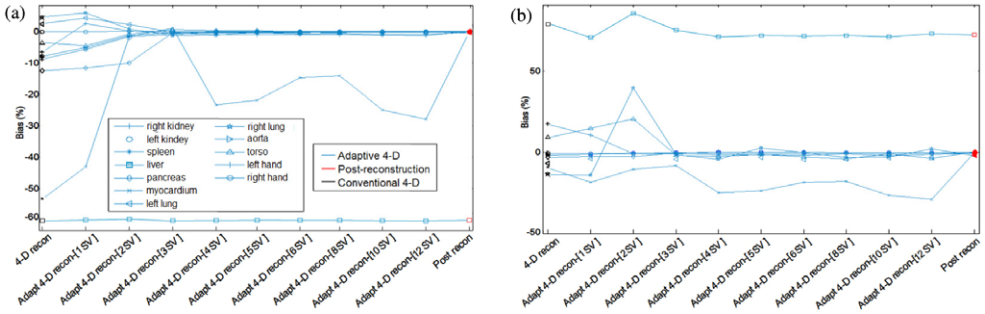

Figure 7. Mean K_1 (*a*) and Vd (*b*) bias for the different parameter estimation methods for all regions of interest in the phantom (complex dataset - noiseless data- 15th iteration). With conventional 4D reconstruction most of the well modelled regions show bias depending on their proximity in badly modelled regions (liver bias ~ 70%). Using the adaptive 4D reconstruction, bias in these regions is greatly reduced as more singular values are used in the secondary model. The post-reconstruction case is shown for comparison with bias only in the poorly modelled region (liver).

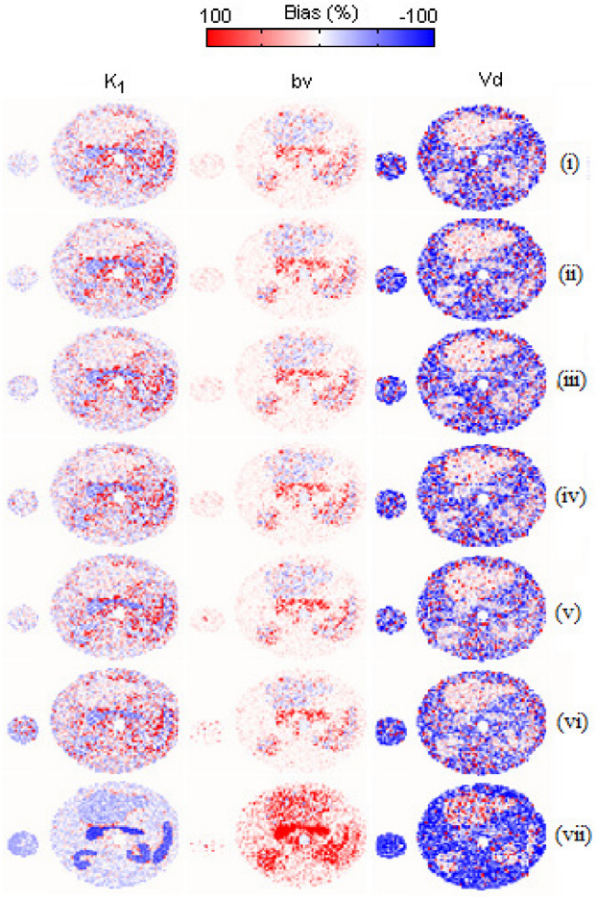

Figure 8. Parametric images of mean bias over the noisy realizations for the simple dataset using conventional 4D image reconstruction (i), the proposed adaptive 4D reconstruction with 1 (ii), 2 (iii), 3 (iv), 5 (v) and 8 (vi) singular values in the secondary model, as well as the post-reconstruction kinetic modelling (vii) (10th iteration).

remains the same in all 4D reconstruction methods and similar to the post-reconstruction analysis since the secondary model in the adaptive 4D method only improves the fit in these regions, with the kinetic parameters still biased due to the erroneous primary model fit.

4.4. Impact of adaptive 4D reconstruction on noise induced bias and the spatial propagation of model induced bias - noisy dataset

Under noisy conditions the behaviour of the different algorithms becomes even more complex. Figure 8 shows parametric images of mean bias over 50 noisy realizations for K_1, blood volume and Vd for the simple dataset, estimated using the conventional 4D reconstruction (i), the post-reconstruction kinetic analysis (vii) and the adaptive 4D reconstruction using a variable number of singular values in the secondary residual model (ii-vi). As reported in (Kotasidis *et al* 2011), the conventional direct 4D method results in substantial improvements in bias compared to the post-reconstruction analysis. Using the adaptive 4D in this dataset, where there are no structured residuals due to erroneous model formulation, and progressively

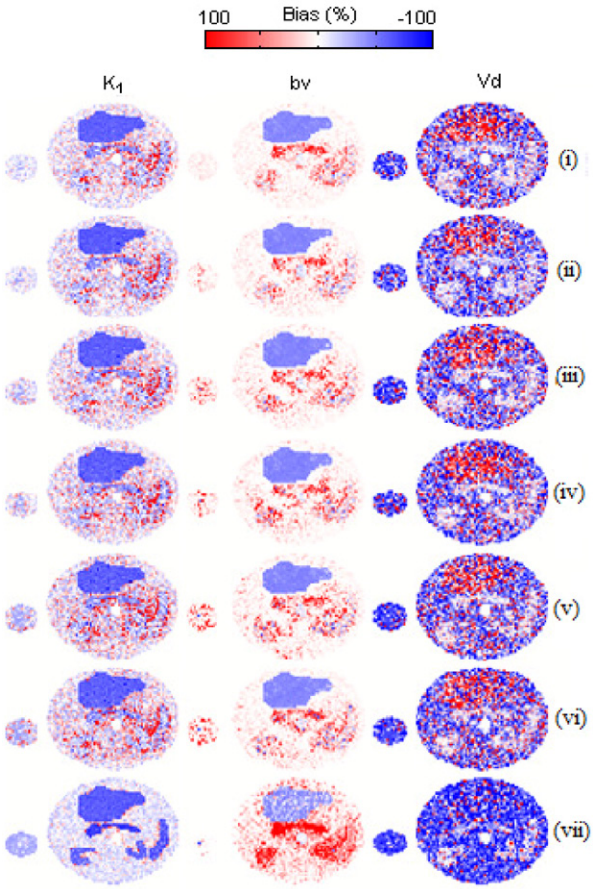

Figure 9. Parametric images of mean bias over the noisy realizations for the complex dataset using conventional 4D image reconstruction (i), the proposed adaptive 4D reconstruction with 1 (ii), 2 (iii), 3 (iv), 5 (v) and 8 (vi) singular values in the secondary model, as well as post-reconstruction kinetic modelling (vii) (10th iteration).

increasing the dimensionality of the secondary model, results in gradually modelling unstructured residuals originating from noise in the data. Putting residuals due to noise back into the dynamic image sequence, gradually increases bias in the kinetic parameter. However even when 8 singular values are used in the adaptive method, the bias in the parameters is still substantially lower compared to the post-reconstruction method and only slightly increased compared to the conventional 4D method.

Moving to the complex dataset where there are structured residuals figure 9 again shows parametric images of mean bias over 50 noisy realizations for K_1, blood volume and Vd estimated using the conventional 4D reconstruction (i), the post-reconstruction kinetic analysis (vii) and the adaptive 4D reconstruction using a variable number of singular values in the secondary residual model (ii-vi). As observed again in (Kotasidis *et al* 2011), even though the conventional 4D reconstruction has lower noise-induced bias compared to the post-reconstruction analysis in well modelled regions, these regions suffer from additional bias spatially propagating from badly modelled regions, reducing the benefits of the direct 4D method. Using the adaptive method, initially, a similar trend is seen as in figure 8, with randomly distributed bias

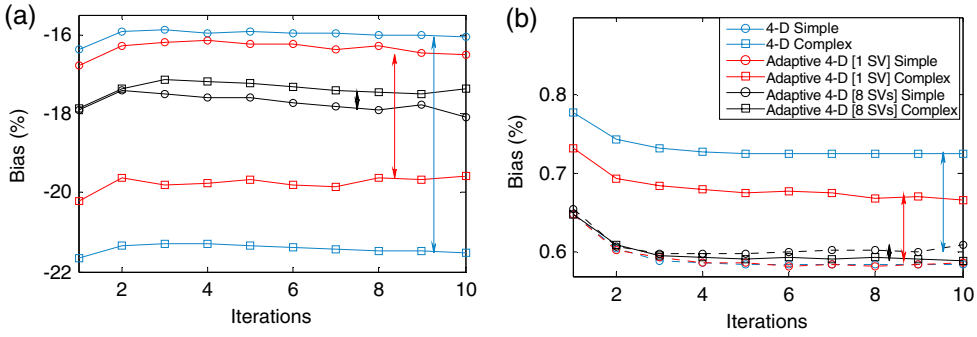

Figure 10. Mean bias as a function of iterations (noisy data) for K_1 (*a*), k_2 (*b*), bv (*c*) and Vd (*d*) for a region of interest covering the entire pancreas (well-modelled region) for both datasets and using the conventional 4D reconstruction as well as the adaptive 4D reconstruction with 1 and 8 singular values in the secondary model.

in the kinetic parameters increasing when increasing the number of SVs. Also based on figure 4 one would expect bias due to propagation to decrease as more singular values are used. As such comparing the bias in a well modelled regions from the simple dataset in figure 8 (noise induced bias) with the bias in the same regions from the complex dataset in figure 9 (noise induced bias + bias due to propagation) can reveal any bias propagation reduction. However it is very difficult to visually compare bias between the 2 datasets, as the magnitude of the bias due to propagation is masked by the noise induced bias and quantitative analysis is needed. In figure 10 K_1 and Vd bias for a well-modelled region (pancreas) is plotted for the simple and the complex datasets, using the adaptive 4D method with 1 and 8 singular values representing the extreme cases, as well as using the conventional 4D method for comparison. Using the conventional 4D reconstruction the bias level seen in the simple dataset is due to noise with the additional bias in the complex dataset due to bias propagation. When the adaptive methods is used with 1 singular value, the K_1 noise induced bias in the simple dataset increases slightly compared to the conventional 4D, but at the same time the additional bias due to propagation has now been reduced looking at the difference with the complex dataset. Using 8 singular values again, a further slight deterioration is seen in the noise induced bias, looking at the simple dataset, due to modelling unstructured residuals from noise. However, bias in the complex data*et al*most coincides with that from the simple dataset, signifying that bias due to propagation has been substantially reduced. In Vd a similar reduction in bias from propagation is observed without any increased bias due to noise as more SVs are used. Although bias, being the index of interest, is overall improved with the adaptive 4D reconstruction due to the reduction in the propagation induced bias outweighing any bias deterioration from noise, variance performance should also be considered. As more SVs are included in the secondary model and random residuals infiltrate back into the dynamic image, variance in the kinetic parameters is not expected to be unaffected. This trend can be seen in figure 11 both for the simple and complex datasets respectively where coefficient of variation (CoV) parametric maps are shown for the different 4D parameter estimation schemes, for a slice through the phantom and at the 10th iteration. When 1 or 2 SVs are used in the adaptive 4D (figure 11(*a*) (ii-iii)), no significant difference is observed in the CoV. However when moving to 8 SVs the parametric maps appear noisier with increased CoV. The same trends is seen in both dataset with no considerable difference between the well modelled regions across the 2 datasets. Since the variance difference is relatively small compared to the variance level in most of the organs, in order to quantify this increase, the mean CoV within the pancreas

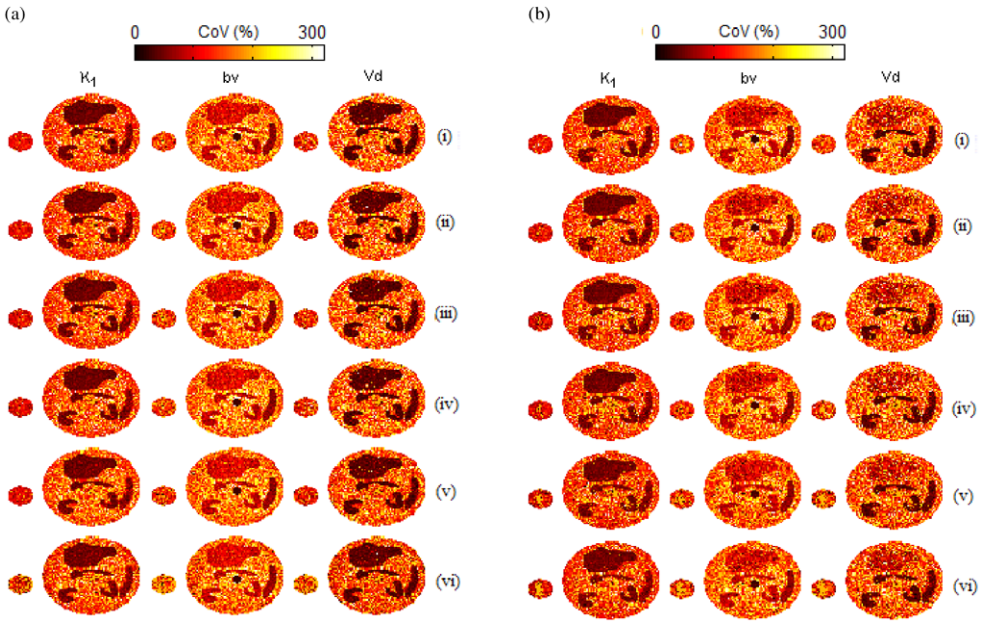

Figure 11. Parametric images of coefficient of variation across the noisy realizations for the (*a*) simple and (*b*) complex dataset using conventional 4D image reconstruction (i) as well as the proposed adaptive 4D reconstruction with 1 (ii), 2 (iii), 3 (iv), 5 (v) and 8 (vi) singular values in the secondary model (10th iteration).

ROI (well modelled region) is plotted for K_1 and Vd as a function of iterations (figure 12(*a*) and (*b*)) for the conventional 4D as well as for 2 adaptive 4D reconstructions corresponding to 2 extreme cases with 1and 8 SVs in the secondary model. Both for K_1 and Vd the CoV deteriorates by almost 3% and 4% respectively in the adaptive 4D method compared to the conventional 4D reconstruction with small differences (<1%) between the 2 datasets (absolute percentage differences).

Evidently then increasing the dimensionality of the secondary model in the adaptive 4D reconstruction leads to reduced bias in the parameter estimates at the expense of increased variance. Using a combined index which takes into account both bias and variance can facilitate a more informative comparison between the 4D parameter estimation schemes. Such a comparison is shown in figure 13 where the root mean square error (RMSE) for an ROI in the pancreas is plotted for all kinetic parameters (K_1, k_2, blood volume and Vd) as a function of iterations. Again data from both datasets are shown in the graphs, reconstructed with the conventional 4D as well as with 2 adaptive 4D reconstructions with 1 and 8 SVs in the secondary model.

The RMSE trend both in K_1 and k_2 is similar, with the difference between the complex and simple datasets reconstructed with the conventional 4D approach reflecting the bias propagating due to the erroneous model formulation mainly in the liver and heart ventricles which are in the vicinity of the pancreas. Looking at the simple dataset and moving to the adaptive 4D method the increase in the RMSE with the number of SVs can be attributed to the combined increase in bias as well as variance due to increased unstructured residuals from noise put back into the dynamic image sequence. However contrary to the simple dataset, in the complex dataset the RMSE is decreasing with the number of SVs as the effect of bias reduction from reduced propagation of the model induced bias on the RMSE, outweighs the

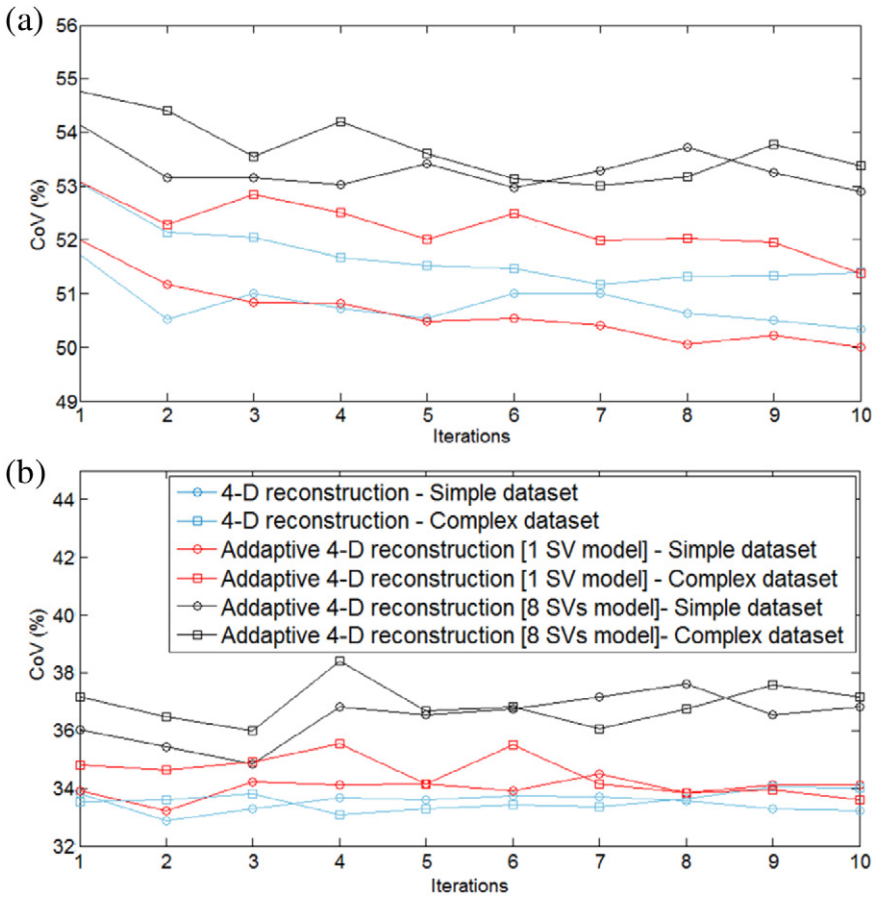

Figure 12. Coefficient of variation as a function of iterations for K_1 (*a*) and Vd (*b*) for a region of interest covering the entire pancreas (well-modelled region) for both datasets and using the conventional 4D reconstruction as well as the adaptive 4D reconstruction with 1 and 8 singular values in the secondary model.

contribution from the increased noise induced bias and variance. When using 8 SVs in the secondary model both datasets converge to similar RMSE estimates. This is due to the fact that in the complex dataset, the bias from propagation and its contribution on the RMSE is reduced matching the RMSE on the simple dataset. However, even though the adaptive 4D with 8 SVs in the complex dataset does improve the RMSE in K_1 and k2, there is still margin for further improvements (still higher RMSE compared to the ideal case of the simple dataset reconstructed with the conventional 4D method) as the propagation induced bias benefits of the adaptive 4D method are partly negated by the unavoidable noise induced bias and variance increase, preventing the adaptive 4D to deliver its full potential. This is not the case on the blood volume parameter as the RMSE in the complex dataset using adaptive 4D with 8 SVs can actually match the RMSE in the simple dataset using the conventional 4D reconstruction. The noise induced bias and variance in the blood volume parameter is mainly unaffected by the small portion of unstructured residuals from noise which managed to go back into the dynamic image in the adaptive 4D. As such the RMSE improvement reflects only the bias propagation improvement of the adaptive 4D method. The opposite is observed in the Vd

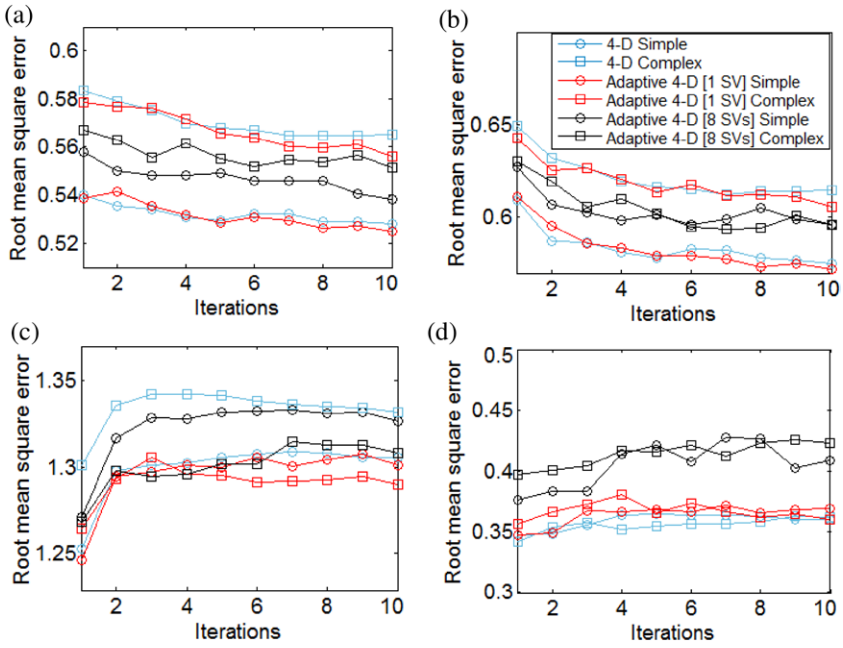

Figure 13. RMSE as a function of iterations for K_1 (*a*), k_2 (*b*), blood volume (*c*) and Vd (*d*) for a region of interest covering the entire pancreas (well-modelled region) for both datasets and using the conventional 4D reconstruction as well as the adaptive 4D reconstruction with 1 and 8 singular values in the secondary model.

where the RMSE deteriorates with the number of SVs as the increase in the noise induced bias and variance from unstructured residuals outweighs the reduction in the propagation induced bias. From figure 3 (v) it can be seen that the bias propagation in the Vd parametric map is not significant compared to K_1 and blood volume. This is also reflected in the RMSE as the difference between the 2 datasets in the conventional 4D is very small signifying small bias propagation with the adaptive 4D only deteriorating the RMSE.

5. Discussion

Methods for direct parameter estimation from measured data in dynamic PET imaging have consistently demonstrated the added benefits of such an approach in generating voxel-wise parametric maps of improved accuracy and precision compared to traditional post-reconstruction kinetic analysis. Provided that the biologic processes in the majority of the imaging FOV are accurately described by the kinetic model, parameters of improved statistical quality can be obtained. However as explained in the Introduction section, this is not the case in body imaging and the variety of kinetics in the FOV doesn't enable the construction of a common kinetic model to describe the temporal distribution of the tracer in the majority of the regions. Erroneous model fits in regions not described by the model can affect the estimated kinetic parameters in adjacent regions for which the model is valid, through propagation of errors during the tomographic step in each iteration. To improve model fits in badly modelled regions in the absence of a single common kinetic model and prevent bias from these regions spatially propagating to well modelled regions, a new approach to direct parametric reconstruction was implemented and evaluated. The method uses a new kinetic modelling strategy, based on the

adaptive inclusion of structured residuals due to erroneous model formulation back into the image. However it has to be emphasized that the adaptive method doesn't affect the kinetic parameters in those erroneously modelled regions estimated during the primary model fit, but only improves the data fit. It is this improved fit in the badly modelled regions in the kinetic modelling step that can prevent bias propagating in the well modelled regions during the tomographic step, indirectly reducing parameter bias in these regions and helping 4D reconstruction deliver its full potential. This is performed by penalising the primary kinetic model with the introduction of a second more general model. To avoid affecting the kinetic parameters in regions for which the primary model is valid, an orthogonality constraint is imposed as detailed in (Matthews *et al* 2012). This results in a 2 step fitting routine with the secondary model applied on the residuals following the application of the primary biological model.

As discussed in (Matthews *et al* 2012), optimizing the penalty weight is important in controlling the inclusion of unstructured residuals from noise back into the dynamic image sequence. This effect is reflected throughout the results in the context of 4D parameter estimation as modelling and including residuals from noise contributes to increased bias and variance in the parametric maps. The number of parameters in the secondary model directly affects this, with more parameters resulting in a larger portion of unstructured residuals being modelled. However optimization of the penalty term using generalized cross validation enables to minimize residuals from noise infiltrating back into the image by reducing the contribution of the included residual when fitting to noise (Matthews *et al* 2012).

In this work we used a data driven approach to construct the secondary model based on sequential increase of the parameters in the model. However, it was observed that there is a trade off between minimizing the bias from propagation and increasing bias and variance through increased noise in the data, as more SVs are used in the secondary model. The aforementioned trade-off also depends on the data itself. In the well modelled regions which are close to the vicinity of erroneously modelled regions and are highly affected, the use of a secondary model is beneficial. As the bias from propagation is relatively high, bias reduction achieved by the use of an adaptive scheme outweighs any increase in bias and variance from increased noise in the data. However, in regions which are further away from the erroneously modelled regions and are not affected from the spatial propagation of bias, using the adaptive method can deteriorate the RMSE as the inclusion of a secondary model increases the noise induced bias and variance without any bias reduction from propagation to outweigh this increase. The same applies to the individual parameters as some are affected more than others through propagation of bias and the success of the adaptive scheme depends on the severity of this bias propagation. In other words when bias from propagation is not significant the penalty from using a secondary model due to increased noise induced bias and variance is higher than any gain from reduction in the propagation of the model induced bias. Having said that, choosing the correct model as well as the number of parameters is paramount for the success of the adaptive 4D scheme. Different secondary models are expected to behave differently in their attempt to describe structured residuals not modelled by the primary model. They also behave differently in their ability to model noise. We observed that using a data driven approach works well for large regions such as the liver but is not optimal for small regions such as the injection site as seen in figure 3, with small bias still propagating around the injection site. Such an effect is in accordance with what has been reported by (Matthews *et al* 2012) as data driven approaches work well when there is a significant number of voxels with similar kinetics not modelled by the primary model. In smaller regions a model with smooth basis functions maybe more appropriate, assuming that any temporal correlation in the residuals indicates biological processes that couldn't be modelled by the primary model. Using then a secondary model which combines both approaches may be better to take into account the different types

of erroneously modelled kinetics in the FOV. Finally the trade-off between noise induced and model induced bias depends also on the simulations used to prove it. In our case we used only emission events without any attenuation, normalization and scatter effects which depending on the tomographic reconstruction used will most likely an effect on the noise induced bias.

6. Conclusion

A new parameter estimation scheme is implemented and evaluated using fully 4D simulated datasets. When diverse and complex kinetics are present in the FOV not described by the primary model, using an adaptive kinetic modelling analysis within a 4D framework enables improved model fitting in these regions and minimizes kinetic parameter error propagation in regions of interest. Using an adaptive 4D scheme improves upon the existing 4D reconstruction methods in the presence of challenging kinetics in the FOV, but careful optimization is required both in the choice of the secondary model and its dimensionality in order to maximize the potentials of the method. Improvements also greatly depend on the vicinity to the erroneously modelled regions and on the severity of the bias propagation. Nevertheless this work proposes a new approach to parameter estimation which based on simulated data allows the benefits of direct spatiotemporal 4D reconstruction to be realized in body imaging. It also open the road for further investigations regarding the choice of an appropriate secondary model and its dependence on the choice of the primary kinetic model as well as the data. The benefits of such an approach on clinical data remain to be seen and is the subject of future investigations.

Acknowledgements

This work was supported by the Swiss National Science Foundation under grants SNSF 31003A-135576 and 31003A-149957.

References

Angelis G I, Matthews J C, Kotasidis F A, Markiewicz P J, Lionheart W R and Reader A J 2014 Evaluation of a direct 4D reconstruction method using generalised linear least squares for estimating nonlinear micro-parametric maps *Ann. Nucl. Med.* 1–14

Feng D, Huang S C, ZhiZhong W and Dino H 1996 An unbiased parametric imaging algorithm for nonuniformly sampled biomedical system parameter estimation *IEEE Trans. Med. Imag.* **15** 512–18

Gravel P and Reader A J 2013 Direct 4D PET MLEM reconstruction of parametric images using the simplified reference tissue model with the basis function method *Nuclear Science Symp. and Medical Imaging Conf. (NSS/MIC), 2013 IEEE*, pp 1–7

Jianhua Y, Planeta-Wilson B and Carson R E 2012 Direct 4-D PET list mode parametric reconstruction with a novel EM algorithm *IEEE Trans. Med. Imag.* **31** 2213–23

Kamasak M E, Bouman C A, Morris E D and Sauer K 2005 Direct reconstruction of kinetic parameter images from dynamic PET data *IEEE Trans. Med. Imag.* **24** 636–50

Kotasidis F A, Matthews J C, Angelis G I, Markiewicz P J, Lionheart W R and Reader A J 2011 Impact of erroneous kinetic model formulation in Direct 4D image reconstruction *Nuclear Science Symp. and Medical Imaging Conf. (NSS/MIC), 2011 IEEE*, pp 2366–7

Kotasidis F A, Matthews J C, Reader A J, Angelis G I, Price P M and Zaidi H 2012 Direct parametric reconstruction for dynamic [^{18}F]-FDG PET/CT imaging in the body *Nuclear Science Symp. and Medical Imaging Conf. (NSS/MIC), 2012 IEEE*, pp 3383–3386

Kotasidis F A, Reader A J, Angelis G I, Markiewicz P J, Walker M D, Price P M, Lionheart W R and Matthews J C 2010 Direct parametric estimation of blood flow in abdominal PET/CT within an EM reconstruction framework *Nuclear Science Symp. Conf. Record (NSS/MIC), 2010 IEEE*, pp 2868–2874

Kudomi N, Slimani L, Jarvisalo M J, Kiss J, Lautamaki R, Naum G A, Savunen T, Knuuti J, Iida H, Nuutila P and Iozzo P 2008 Non-invasive estimation of hepatic blood perfusion from H_2 ^{15}O PET images using tissue-derived arterial and portal input functions *Eur. J. Nucl. Med. Mol. Imaging* **35** 1899–911

Matthews J, Bailey D, Price P and Cunningham V 1997 The direct calculation of parametric images from dynamic PET data using maximum-likelihood iterative reconstruction *Phys. Med. Biol.* **42** 1155–73

Matthews J C, Angelis G I, Kotasidis F A, Markiewicz P J and Reader A J 2010 Direct reconstruction of parametric images using any spatiotemporal 4D image based model and maximum likelihood expectation maximisation *Nuclear Science Symp. Conf. Record (NSS/MIC), 2010 IEEE*, pp 2435–41

Matthews J C, Reader A J, Angelis G I, Price P M, Markiewicz P J and Kotasidis F A 2012 Adaptive parametric kinetic modelling for improved full field of view fitting of PET data *Nuclear Science Symp. and Medical Imaging Conf. (NSS/MIC), 2012 IEEE*, pp 3925–9

Merlin T, Fernandez P, Visvikis D and Lamare F 2013 Direct 4D patlak parametric image reconstruction algorithm integrating respiratory motion correction for oncology studies *Nuclear Science Symp. and Medical Imaging Conf. (NSS/MIC), 2013 IEEE*, pp 1–6

Rahmim A, Lodge M, Tang J, Zhou Y, Hussain B, Wong D, Pili R and Wahl R 2010 Dynamic FDG PET imaging using direct 4D parametric reconstruction in cancer patients *J. Nucl. Med. Meet. Abstr.* **51** 354

Rahmim A, Tang J and Mohy-ud-Din H 2014 Direct 4D parametric imaging in dynamic myocardial perfusion PET *Front. Biomed. Technol.* **1** 4–13

Rahmim A, Tang J, Mohy-ud-Din H, Ay M and Lodge M 2011 Use of optimization transfer for enhanced direct 4D parametric imaging in myocardial perfusion PET *J. Nucl. Med. Meet. Abstr.* **52** 265

Rahmim A, Tang J and Zaidi H 2009 Four-dimensional (4D) image reconstruction strategies in dynamic PET: beyond conventional independent frame reconstruction *Med. Phys.* **36** 3654–70

Rahmim A, Zhou Y, Tang J, Lu L, Sossi V and Wong D F 2012 Direct 4D parametric imaging for linearized models of reversibly binding PET tracers using generalized AB-EM reconstruction *Phys. Med. Biol.* **57** 733–55

Rakvongthai Y, Ouyang J, Guerin B, Li Q, Alpert N M and El Fakhri G 2013 Direct reconstruction of cardiac PET kinetic parametric images using a preconditioned conjugate gradient approach *Med. Phys.* **40** 102501

Reader A J, Sureau F C, Comtat C, Trebossen R and Buvat I 2006 Joint estimation of dynamic PET images and temporal basis functions using fully 4D ML-EM *Phys. Med. Biol.* **51** 5455–74

Su K H, Yen T C and Fang Y H 2013 A novel approach for direct reconstruction of parametric images for myocardial blood flow from PET imaging *Med. Phys.* **40** 102505

Tang J, Kuwabara H, Wong D F and Rahmim A 2010 Direct 4D reconstruction of parametric images incorporating anato-functional joint entropy *Phys. Med. Biol.* **55** 4261–72

Tsoumpas C, Turkheimer F E and Thielemans K 2008 Study of direct and indirect parametric estimation methods of linear models in dynamic positron emission tomography *Med. Phys.* **35** 1299–309

Wang G, Fu L and Qi J 2008 Maximum a posteriori reconstruction of the Patlak parametric image from sinograms in dynamic PET *Phys. Med. Biol.* **53** 593–604

Wang G and Qi J 2009 Generalized algorithms for direct reconstruction of parametric images from dynamic PET data *IEEE Trans. Med. Imaging* **28** 1717–26

Wang G and Qi J 2010 Acceleration of the direct reconstruction of linear parametric images using nested algorithms *Phys. Med. Biol.* **55** 1505–17

Wang G and Qi J 2012 An optimization transfer algorithm for nonlinear parametric image reconstruction from dynamic PET data *IEEE Trans. Med. Imaging* **31** 1977–88